

Effect of electron heating on femtosecond laser-induced coherent acoustic phonons in noble metals

Jincheng Wang and Chunlei Guo*

The Institute of Optics, University of Rochester, Rochester, New York 14627, USA

(Received 20 December 2006; revised manuscript received 24 April 2007; published 15 May 2007)

We employ a surface plasmon technique to resolve the dynamics of femtosecond-laser-induced coherent acoustic phonons in noble metals. Clear acoustic oscillations are observed in our experiments. We further study the dependence of the initial phase of the oscillations on pump fluence, and we find that the initial phase decreases linearly with pump fluence. Our model calculations show that hot electrons instantaneously excited by femtosecond pulses contribute to the generation of coherent acoustic phonons in metals.

DOI: [10.1103/PhysRevB.75.184304](https://doi.org/10.1103/PhysRevB.75.184304)

PACS number(s): 63.20.-e, 63.20.Kr, 78.47.+p, 73.20.Mf

Coherent acoustic phonons in solid materials generated by impulsive optical excitation have been extensively studied in the past.¹⁻⁹ Impulsive stimulated Brillouin scattering¹ (ISBS) and impulsive stimulated thermal scattering^{2,3} (ISTS) are two main mechanisms that lead to the generation of coherent acoustic phonons in solids. Ultrashort pulse lasers have been demonstrated as a unique tool in generating coherent acoustic phonons in thin films and nanoparticles,^{4,5} where the pressure from hot electrons has been suggested as an important factor in driving the coherent acoustic phonons in metals. The change of material reflectance or transmittance due to acoustic phonons is usually very small, and the detection often requires a phase-sensitive detection instrument (e.g., a lock-in amplifier) combined with a high-repetition-rate laser system [e.g., a femtosecond (fs) oscillator running at tens of MHz repetition rate] to yield a high signal-to-noise ratio. Since the signal-to-noise ratio increases with laser repetition rate for phase-sensitive detection, direct monitoring of reflectance or transmittance is usually not suitable for detecting acoustic phonons when a low-repetition-rate laser system is used (e.g., a 1-kHz fs amplifier⁶). Techniques such as third-harmonic detection,⁶ transient grating measurement,⁷ x-ray or electron pulse diffraction,^{5,8} and angular deflection of light⁹ have been used to enhance the sensitivity of acoustic phonon detection.

The study of surface plasmons (SPs) has shown that SPs can be used as a powerful spectroscopic tool in detecting small changes in material dielectric constants.¹⁰⁻¹³ A surface plasmon is an energy wave coupled with a collective electron-density oscillation on a metal-dielectric interface, decaying evanescently on both sides of the interface.¹⁴ SPs can be readily generated optically using a Kretschmann configuration.¹⁵ Previously, the SP technique has been used to resolve the dynamics of coherent acoustic phonons in Ag film.¹⁶ However, the role of electron heating in driving coherent acoustic phonons could not be studied in that work due to the longer laser pulses (ps) used.¹⁶ In this work, we employ the surface plasmon technique to detect acoustic phonons in noble-metal (Au and Cu) films following low-repetition-rate fs-laser-pulse excitation. We choose the noble metals because their onset interband transition energy (~ 2.5 eV for both Au and Cu) is greater than the photon energy used in our experiment (1.55 eV). Therefore, our fs laser pulses excite electrons in a metal through pure ultrafast heating rather than more complicated interband transitions.

The effects of hot-electron pressure on the generation of coherent acoustic phonons are studied in this paper.

The experiment uses an amplified Ti:sapphire fs laser system that generates 66-fs pulses about 1 mJ/pulse at a 1-kHz repetition rate with the central wavelength at 800 nm. The samples used in our experiment are a 50-nm Au film and a 40-nm Cu film. The metal films are coated on 1-mm-thick glass substrates (BK7) with *e*-beam evaporation. As shown in the inset of Fig. 1, the glass substrate is attached onto a right-angle prism (BK7) with the metal side exposed to the air. Refractive index-matching fluid ($n=1.51$) is placed between the glass substrate and the prism such that the metal film can be thought of being directly coated onto the prism. The prism is used to launch SPs along the air-metal interface through the Kretschmann configuration,¹⁵ where a *p*-polarized beam is incident from the back side of the metal film (glass-metal interface). The SP-resonance angle for each sample is first determined by measuring the dependence of reflectance on the angle of incidence. Figure 1 shows the results of Au and Cu, and the minimum reflectance corresponds to the SP-resonance angle for each sample. The width of the resonance angle curve observed in our experiment

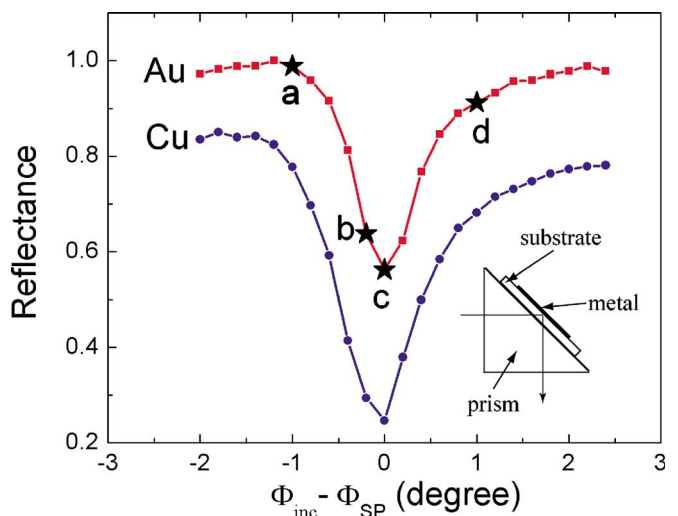


FIG. 1. (Color online) The dependence of light reflectance on the incident angle (Φ_{inc}) in the vicinity of the SP-resonance angle (Φ_{sp}) for Au and Cu. The Cu curve is offset for visual clarity. The stars on the Au curve mark four probe incident angles where pump-probe data are taken in Fig. 2. The inset shows the probe geometry.

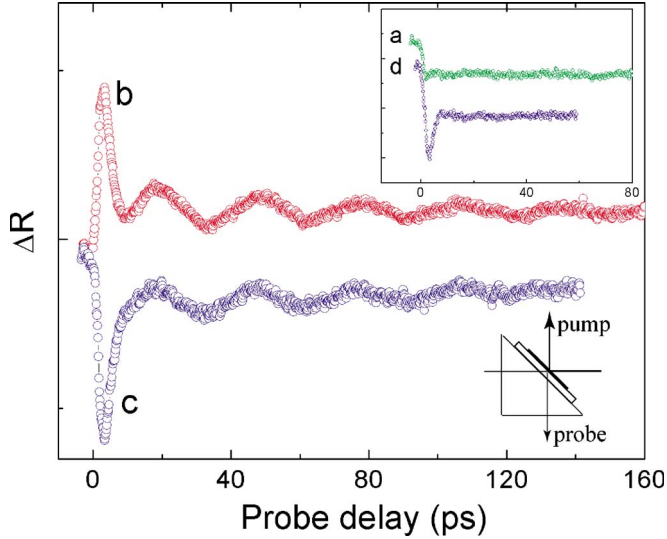


FIG. 2. (Color online) Pump-probe reflectance signal of Au for the probe beam incident at angles both off the SP resonance (curves *a* and *d* in the upper inset) and near the SP resonance (curves *b* and *c*). The label for each curve corresponds the incident angle (marks in Fig. 1), at which the data are taken. The lower inset shows the pump-probe experiment setup.

($\sim 1^\circ$) is broader than the calculated curve based on a single wavelength ($\sim 0.2^\circ$ at 800 nm). We believe this is due to the fact that our fs pulses have a broad spectral bandwidth.

As shown in the lower inset of Fig. 2, we generate coherent acoustic phonons by heating the front metal surface with a weakly focused *p*-polarized pump beam ($\sim 0.7 \mu\text{m}$ in diameter). Pump-induced optical property changes in the metal film are probed by the probe beam from the back metal surface. The area of the pump beam on the sample surface is more than 10 times larger than that of the probe beam. Figure 2 shows the pump-probe reflectance measurements for Au with pump fluence $\sim 4 \text{ mJ/cm}^2$ and at four different probe angles that are either off the SP resonance (marks *a* and *d* in Fig. 1) or near the SP resonance (marks *b* and *c* in Fig. 1). The reflectance change ΔR shows a sharp change immediately following pump excitation due to the initial hot-electron generation and subsequent electron-phonon thermalization. As shown by curves *a* and *d* in the upper inset of Fig. 2(a), for probe beam incidents at an angle about 1° off the SP-resonance angle, the initial change of ΔR decays monotonously to a near-constant value, indicating that electrons and the lattice reach a thermal equilibrium. However, for the probe beam incident at or near the SP-resonance angle, a periodic oscillation is clearly seen in the ΔR signal, as shown by curves *b* and *c* in Fig. 2(b). The period T of the signal oscillation is ~ 29.5 ps. These oscillations are believed due to a pump-induced coherent acoustic phonon [one-dimensional (1D) standing strain wave] in the Au film. The calculated velocity of the acoustic phonons in our Au film is 3.39 km/s using $L=50$ nm and $T=29.5$ ps, which agrees well the sound velocity of 3.24 km/s in bulk gold.¹⁷ Therefore, our experimental results show that the sensitivity of detecting coherent acoustic phonons is greatly enhanced when SP is involved in the probe beam that is incident near the SP resonance angle.

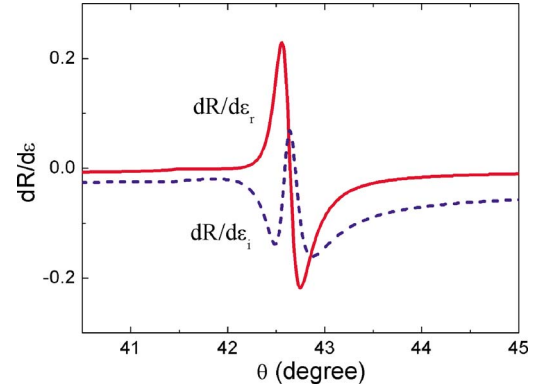


FIG. 3. (Color online) Calculated rate of changes of reflectance on Au with respect to dielectric constant at different incident angles for back-surface probe ($dR/d\varepsilon_r$, solid line, and $dR/d\varepsilon_i$, dashed line). The calculations are based on a 50-nm Au film with 800-nm irradiation.

This enhanced sensitivity of the SP probe can be understood by considering the change of reflectance R with respect to both the real (ε_r) and imaginary (ε_i) parts of dielectric constant, given by

$$\Delta R = \frac{dR}{d\varepsilon_r} \Delta\varepsilon_r + \frac{dR}{d\varepsilon_i} \Delta\varepsilon_i, \quad (1)$$

where $\Delta\varepsilon_r$ and $\Delta\varepsilon_i$ are due to pump excitation while $dR/d\varepsilon_r$ and $dR/d\varepsilon_i$ are determined by the probe properties. A certain pump excitation will induce a fixed amount of $\Delta\varepsilon_r$ and $\Delta\varepsilon_i$, and the probe signal strength will then be determined by $dR/d\varepsilon_r$ and $dR/d\varepsilon_i$. For a probe beam incident onto a metal film from the back side, the reflectance is given as follows for a three-layer (glass/metal/air) system:¹³

$$R(\theta, \varepsilon, d) = \left| \frac{r_{01}(\theta, \varepsilon) + r_{12}(\theta, \varepsilon) e^{2ik_{z1}(r_{12}(\theta, \varepsilon) d)}}{1 + r_{01}(\theta, \varepsilon) r_{12}(\theta, \varepsilon) e^{2ik_{z1}(r_{12}(\theta, \varepsilon) d)}} \right|^2, \quad (2)$$

with

$$r_{ik} = \left(\frac{k_{zi}}{\varepsilon_i} - \frac{k_{zk}}{\varepsilon_k} \right) / \left(\frac{k_{zi}}{\varepsilon_i} + \frac{k_{zk}}{\varepsilon_k} \right),$$

where θ is the incident angle, ε is the dielectric constant of a metal film, and d is the thickness of a metal film. r_{01} and r_{12} represent the reflectivity of the glass/metal and metal/air interfaces, respectively. Based on Eq. (2), the dependence of $dR/d\varepsilon_r$ and $dR/d\varepsilon_i$ on the incident angle for back surface probes is calculated and shown in Fig. 3. We can see that the values of $dR/d\varepsilon_r$ and $dR/d\varepsilon_i$ are dramatically enhanced for the probe around the SP resonance angle: the values are on the order of 0.15–0.25 around the SP resonance, but drop significantly off the SP resonance to the values comparable to those of a simple metal-air interface predicted by the regular Fresnel formula ($dR/d\varepsilon_r \sim -2 \times 10^{-3}$ and $dR/d\varepsilon_i \sim -3 \times 10^{-2}$).

We further study the dependence of acoustic phonon oscillation on pump fluence. For a probe beam incident at an angle corresponding to point *b* in Fig. 1, Fig. 4 shows the pump-probe data of Au at different pump fluences. As we

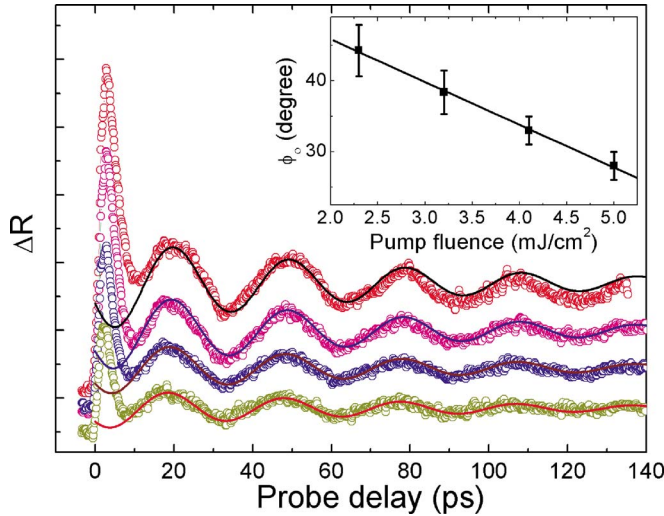


FIG. 4. (Color online) Pump-probe data of Au at different pump fluences. The pump fluence for the data curve is, from top to bottom, 5 mJ/cm², 4.1 mJ/cm², 3.2 mJ/cm², and 2.3 mJ/cm², respectively. The solid lines are data fitting using $Ae^{-t/T_0} \sin(\omega t + \phi_0)$. The inset shows the dependence of the initial phase ϕ_0 on the pump fluence. Error bars are obtained from the nonlinear least-squares fitting to the measured data.

can see from the figure, the magnitude of the initial peak and the following acoustic oscillations increase with pump fluence. The acoustic oscillations at different pump fluence are fitted with a damping sinusoidal function $Ae^{-t/T_0} \sin(\omega t + \phi_0)$, where $\omega = 2\pi/T$ is the angular frequency and T the oscillation period. The amplitude A , the damping constant T_0 , the angular frequency ω , and the initial phase ϕ_0 are determined from data fitting. The damping sinusoidal functions give an excellent fit to our experimental data, as shown by the solid lines in Fig. 4, except, of course, the very beginning of the curves where hot electrons and the lattice are in a thermal nonequilibrium distribution. The fitting results show that the initial phase ϕ_0 is not a constant for different pump fluence. As we can see from the inset of Fig. 4, the initial phase of the acoustic oscillations decreases from $\sim 44^\circ$ to $\sim 28^\circ$ when the incident pump fluence increases from 2.3 mJ/cm² to 5 mJ/cm². It can be seen from the inset of Fig. 4 that ϕ_0 versus pump fluence shows an excellent linear dependence. Similar pump-probe experiments are also performed on Cu. For a probe beam incident at an angle near the SP resonance, coherent acoustic oscillations are also clearly observed on Cu with an oscillation period of $T \sim 17.5$ ps, as shown in Fig. 5. The calculated velocity of the acoustic pulse in Cu film is 4.57 km/s, which also shows good agreement with the sound velocity in bulk Cu at 4.76 km/s.¹⁷ Similar to Au, the initial phase of the acoustic oscillations in Cu also depends on pump fluence. The inset of Fig. 5 shows the extracted ϕ_0 versus pump pulse energy. As we can see, ϕ_0 decreases from 43.0° to 10.4° when the pump fluence increases from ~ 0.92 mJ/cm² to ~ 2.3 mJ/cm² and, once again, ϕ_0 versus pump fluence shows a linear dependence.

The metal samples used in our experiment are thinner than the electron diffusion depth¹⁸ (~ 100 nm for Au and Cu) and, thus, electron thermal diffusion should play a significant

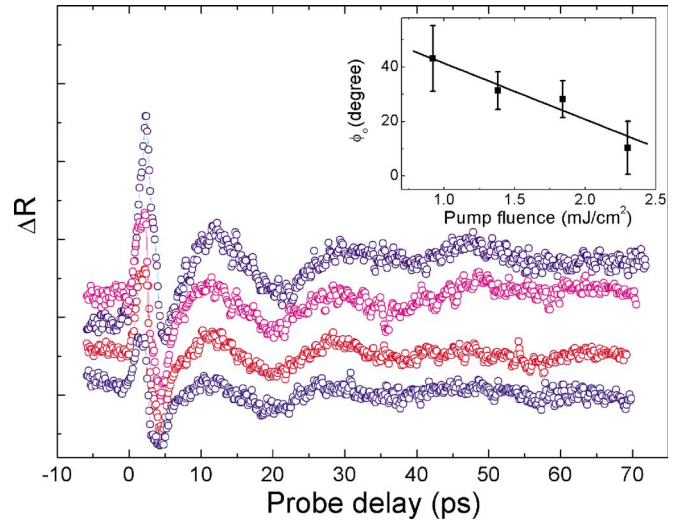


FIG. 5. (Color online) Pump-probe data of Cu at different pump fluences. The pump fluence for the data curve is, from top to bottom, 2.3 mJ/cm², 1.84 mJ/cm², 1.38 mJ/cm², and 0.92 mJ/cm², respectively. The inset shows the dependence of the initial phase ϕ_0 on the pump fluence. Error bars are obtained from the nonlinear least-squares fitting to the measured data.

role during fs laser heating of thin metal films. Using the two-temperature model (TTM),^{19,20} our calculations taking into account electron thermal diffusion show that electrons will thermalize uniformly across the sample depth within 200 fs for a 50-nm Au film. Within this short time scale, the lattice can be regarded staying as an unperturbed system. Therefore, the thermalization process of an entire metal film of ~ 50 nm can be regarded as nearly uniform heating due to the fast electron thermal diffusion and safely described by the TTM. Also, since our pump beam dimension (~ 0.7 μm) is much larger than the film thickness, the generated coherent acoustic phonons (or strain wave) can be treated as a 1D longitudinal standing sound wave as a breathing mode normal to the metal surface. For ultrafast pulse heating of a thin and small solid sample, two mechanisms can contribute to the generation of coherent acoustic phonons.^{4,5,8} One is from the fast thermalized hot electrons in a metal^{4,5} or free carriers in a semiconductor,⁸ which provides an instantaneous stress. Another contribution is a slowly developing lattice thermal stress from electron-phonon coupling.^{5,8}

The dynamics of coherent acoustic phonons in a thin metal film generated via fs pulse heating can be described by a damped harmonic oscillator driven by the thermal stress as^{4,5}

$$\frac{dQ^2}{dt^2} + 2\beta \frac{dQ}{dt} + \omega_0^2 Q = \sigma(t), \quad (3)$$

where ω_0 is the phonon angular frequency and β is a phenomenological damping constant. Thermal stress σ consists of both lattice and electron contributions, and its value at a certain lattice and electron temperature T_e and T_l can be expressed as^{4,5}

$$\sigma = \sigma_l + \sigma_e = -\gamma_l \int_{T_0}^{T_l} C_l dT_l - \gamma_e \int_{T_0}^{T_e} C_e dT_e, \quad (4)$$

where C_l and C_e are the lattice and electron heat capacity, γ_l and γ_e are the lattice and electronic Gruneisen parameters, T_0 is the initial temperature, and T_l and T_e are lattice and electron temperatures and their values can be obtained from calculations of the TTM. Once the time evolution of T_e , T_l , and the acoustic phonon field (Q) are obtained, we apply these values to fit our experimental measurements (ΔR). It has been widely used in studying acoustic phonons that the change of probe beam is proportional to the amplitude of acoustic vibration.^{4,5} Therefore, we also approximate ΔR as linearly dependent on T_e , T_l , and Q ,⁴ and three weighting parameters for T_e , T_l , and Q are used to adjust the calculation amplitude to match the experimental results. We fit the experimental data by setting the peak of the calculated curve to coincide with the peak position of the measured data. Figure 5 shows the fit with measured data at different pump fluence, where the dashed line is the fit by summing T_e , T_l , and the phonon field Q driven only by lattice thermal stress σ_l , and the solid line is the fit by summing T_e , T_l , and the phonon field Q driven by both σ_e and σ_l . We can see from the figure that the initial decrease in reflectance (<9 ps) can be reproduced well by our fitting regardless whether electron thermal stress σ_e is considered or not, since this initial reflectance change is mainly determined by the initial electron-lattice temperature thermalization. However, for the oscillating reflectance signal at the longer time scale (>9 ps) induced by coherent acoustic phonons, the model including both σ_e and σ_l always gives a better fit to the measured data than that considering σ_l alone at various pump fluences, as shown in Fig. 6. Similarly, we find that the inclusion of electron thermal stress will also yield a better fit to the Cu data. Our results support previous studies that hot-electron pressure plays a role in the dynamics of coherent acoustic phonons generated by fs pulse excitation.^{4,5,21} Finally, the initial phase change of the oscillating signal with pump fluence as observed in our experiment can be reproduced by our model calculations. In our experiment, the initial phase of the acoustic oscillation for Au decreases by about 16.3° when the pump fluence increases from 2.3 mJ/cm² to 5 mJ/cm². In our model calculations for Au, the initial phase of the acoustic phonon field decreases by about 13.5° with the same pump fluence change in a linear fashion. Therefore, our model calculations agree well with our experimental results. The dependence of the initial phase on the pump fluence can be understood as follows. At different pump fluences, it takes different times for electrons and lattice to reach thermal equilibrium, and this will lead to different temporal evolutions

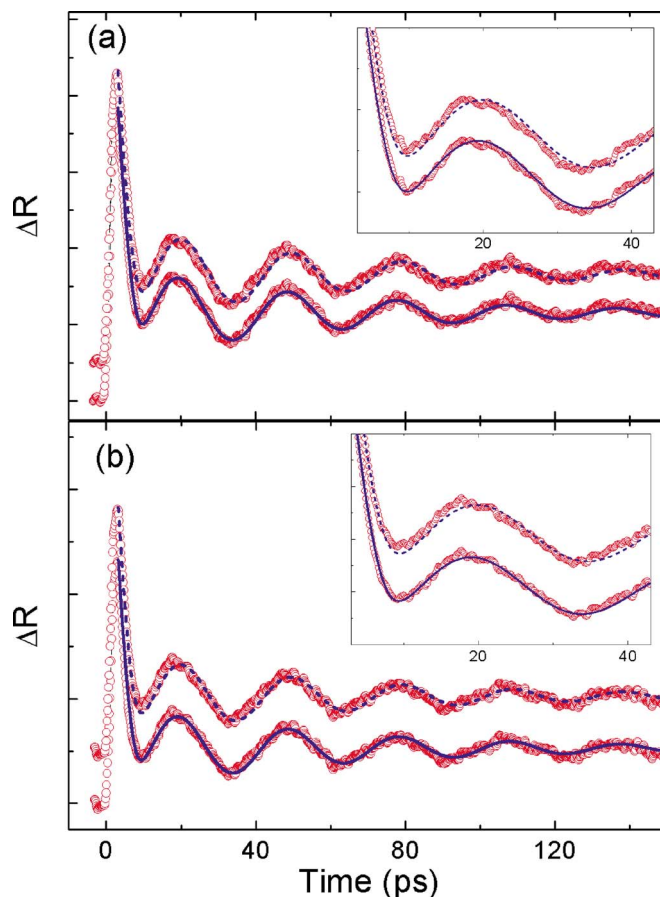


FIG. 6. (Color online) Data and fitting for Au at pump fluence of (a) 4.1 mJ/cm² and (b) 3.2 mJ/cm². The solid lines are data fitting including both σ_e and σ_l , while the dashed line is data fitting including only σ_l . In each figure, two data curves are identical experimental data but offset for visual clarity for the data fitting.

for the development of electron and lattice thermal stress and the subsequent acoustic oscillations.

In summary, we employ a surface plasmon technique to resolve the dynamics of fs-laser-induced coherent acoustic phonons in noble metals. Clear acoustic oscillations are observed in our experiments. We further study the dependence of the initial phase of the oscillations on pump fluence, and we find that the initial phase decreases linearly with the pump fluence. Our study suggests that it is necessary to consider hot-electron pressure to understand the dynamics of coherent acoustic phonon generation by fs-pulse excitation.

The work was supported by the National Science Foundation and the Air Force Office of Scientific Research.

*Electronic address: guo@optics.rochester.edu

¹L. T. Cheng and K. A. Nelson, Phys. Rev. B **37**, 3603 (1988).

²H. J. Maris, Sci. Am. (Int. Ed.) **278** (1), 86 (1998).

³K. A. Nelson and M. D. Fayer, J. Chem. Phys. **72**, 5202 (1980).

⁴M. Perner, S. Gresillon, J. März, G. von Plessen, J. Feldmann, J. Porstendorfer, K.-J. Berg, and G. Berg, Phys. Rev. Lett. **85**, 792

(2000).

⁵H. Park, X. Wang, S. Nie, R. Clinite, and J. Cao, Phys. Rev. B **72**, 100301(R) (2005).

⁶C. Guo and A. J. Taylor, Phys. Rev. B **64**, 245106 (2001).

⁷K. A. Nelson, D. R. Lutz, M. D. Fayer, and L. Madison, Phys. Rev. B **24**, 3261 (1981).

- ⁸A. M. Lindenberg, I. Kang, S. L. Johnson, T. Missalla, P. A. Heimann, Z. Chang, J. Larsson, P. H. Bucksbaum, H. C. Kapteyn, H. A. Padmore, R. W. Lee, J. S. Wark, and R. W. Falcone, *Phys. Rev. Lett.* **84**, 111 (2000).
- ⁹O. B. Wright, *Phys. Rev. B* **49**, 9985 (1994).
- ¹⁰B. Lamprecht, J. R. Krenn, A. Leitner, and F. R. Aussenegg, *Phys. Rev. Lett.* **83**, 4421 (1999).
- ¹¹T. Tsang, T. Srinivasan-Rao, and J. Fischer, *Phys. Rev. B* **43**, 8870 (1991).
- ¹²W. L. Barnes, A. Dereux, and T. W. Ebbesen, *Nature (London)* **424**, 824 (2003).
- ¹³K. Katayama, T. Sawada, Q. Shen, and A. Harata, *Phys. Rev. B* **58**, 8428 (1998).
- ¹⁴H. Raether, *Springer Tracts Mod. Phys.* **111**, 1 (1988).
- ¹⁵E. Kretschmann, *Z. Phys.* **241**, 313 (1971).
- ¹⁶M. van Exter and A. Lagendijk, *Phys. Rev. Lett.* **60**, 49 (1988).
- ¹⁷D. R. Lide, *CRC Handbook of Chemistry and Physics*, 82nd ed. (Chemical Rubber Company, Boca Raton, FL, 2002).
- ¹⁸S. D. Brorson, J. G. Fujimoto, and E. P. Ippen, *Phys. Rev. Lett.* **59**, 1962 (1987).
- ¹⁹M. I. Kaganov, I. M. Lifshitz, and L. V. Tanatarov, *Zh. Eksp. Teor. Fiz.* **31**, 232 (1956) [*Sov. Phys. JETP* **4**, 173 (1957)].
- ²⁰J. K. Chen and J. E. Beraun, *Numer. Heat Transfer, Part A* **40**, 1 (2001).
- ²¹G. V. Hartland, *J. Chem. Phys.* **116**, 8048 (2002).